Kinetic Effect of Local pH on High-Voltage Aqueous Sodium-Ion Batteries

NAKAMOTO, Kosuke
Institute for Materials Chemistry and Engineering, Kyushu University

TANAKA, Miu
Interdisciplinary Graduate School of Engineering Sciences, Kyushu University

SAKAMOTO, Ryo
Institute for Materials Chemistry and Engineering, Kyushu University

ITO, Masato
Institute for Materials Chemistry and Engineering, Kyushu University

他

出版情報：Electrochemistry. 92 (1), pp.017003-, 2024-01-26. 電気化学会
バージョン：

Electrochemistry
The Electrochemical Society of Japan
Received: October 31, 2023
Accepted: December 10, 2023
Published online: December 12, 2023
Issued: January 26, 2024
https://doi.org/10.5796/electrochemistry.23-00124
https://doi.org/10.50892/data.electrochemistry.24785661
Article
Electrochemistry, 92(1), 017003 (2024)

Kinetic Effect of Local pH on High-Voltage Aqueous Sodium-Ion Batteries†

Kosuke NAKAMOTO,[a,*,§] Miu TANAKA,[b] Ryo SAKAMOTO,[a,§]
Masato ITO,[a,*] and Shigeto OKADA[a,*,§§]

[a] Institute for Materials Chemistry and Engineering, Kyushu University, 6-1 Kasuga-Koen, Kasuga, Fukuoka 816-8580, Japan
[b] Interdisciplinary Graduate School of Engineering Sciences, Kyushu University, 6-1 Kasuga-Koen, Kasuga, Fukuoka 816-8580, Japan

* Corresponding authors: nakamoto@cm.kyushu-u.ac.jp (K. N.), ito.masato.795@m.kyushu-u.ac.jp (M. I.), okada.shigeto.893@m.kyushu-u.ac.jp (S. O.)

ABSTRACT

The local pH values in the close vicinity of the cathode/anode were experimentally determined to be strongly acidic/weakly basic, respectively, during the operation of a high-voltage aqueous sodium-ion battery with Prussian blue-type electrodes and a concentrated aqueous electrolyte. The observed pH gradient was ascribed to O_2/H_2 evolution at the cathode/anode in aqueous cells, which should contribute to the expansion of the electrochemical window if the pH gradient is maintained. An increase in the distance between the cathode and anode proved to be one of possible solution to suppress the undesired pH neutralization. On the other hand, the reduction of water as well as the dissolved O_2 in the electrolyte may diminish the capacity of the anode by a self-discharge. This became more pronounced if the full cell was left to stand for a longer time after charging.

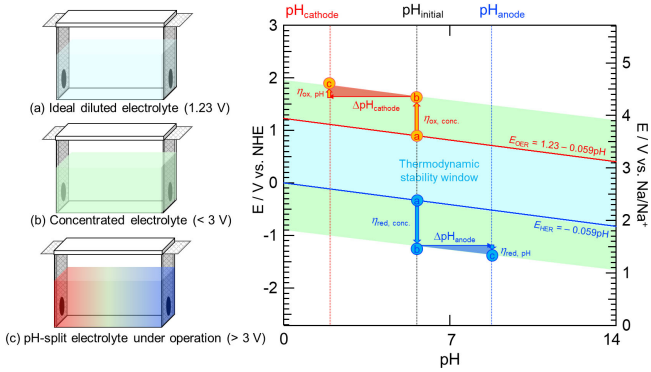

Keywords : pH Gradient, Aqueous Battery, High Voltage, Self-discharge

1. Introduction

Recently, aqueous batteries have attracted attention as essential devices for large-scale energy storage with safety and cost-effectiveness.[1,2] In principle, the voltage of an aqueous battery is thermodynamically limited to less than 1.23 V because water electrochemically decomposes into O_2 and H_2 as shown in the following equations:

Oxygen evolution reaction (OER):

$$2H_2O \rightarrow O_2 + 4H^+ + 4e^- \quad (1)$$

Hydrogen evolution reaction (HER):

$$2H_2O + 2e^- \rightarrow H_2 + 2OH^- \quad (2)$$

The pH values of the ideal diluted solution give the thermodynamic OER/HER potentials as follows:

$$E_{OER} = 1.23 - 0.059pH \quad (\text{vs. NHE}) \quad (3)$$

$$E_{HER} = \quad - 0.059pH \quad (\text{vs. NHE}) \quad (4)$$

In contrast, the electrolysis of water may be kinetically suppressed in the case of highly concentrated aqueous electrolytes. In fact, many aqueous batteries display an operational voltage of over 2 V.[3–6] It is generally accepted that the anion crowding layer prevents the access of water to the cathode,[7] and that anion-derived solid electrolyte interfaces insulate the conduction between water and the anode in these batteries.[8] These factors overall serve to shift the upper ($E_{ox,\,conc.}$) and lower ($E_{red,\,conc.}$) limits of the stability window as follows ($\eta_{ox,\,conc.}/\eta_{red,\,conc.}$ are overpotentials for O_2/H_2 evolution, respectively):

$$E_{ox,\,conc.} = E_{OER} + \eta_{ox,\,conc.} \quad (5)$$

$$E_{red,\,conc.} = E_{HER} - \eta_{red,\,conc.} \quad (6)$$

However, the electrolysis of water becomes non-negligible even with concentrated aqueous electrolytes at $E_{ox,\,conc.}$ and $E_{red,\,conc.}$; therefore, high-voltage aqueous batteries often cause O_2/H_2 gas evolution with concomitant H^+/OH^- accumulation upon operation.[9,10] Now let us define $pH_{initial}$ as the global pH value before operation, and $pH_{cathode}/pH_{anode}$ as the local pH values in the close vicinity of the cathode and anode under operation. Additional overpotentials ($\eta_{ox,\,pH}/\eta_{red,\,pH}$) induced by the pH shifts upon operation[11] are expressed in the following equations:

$$\eta_{ox,\,pH} = -0.059(pH_{initial} - pH_{cathode}) = -0.059\Delta pH_{cathode} \quad (7)$$

$$\eta_{red,\,pH} = -0.059(pH_{initial} - pH_{anode}) = -0.059\Delta pH_{anode} \quad (8)$$

Accordingly, the upper ($E_{ox,\,pH}$) and lower ($E_{red,\,pH}$) limits of the practical stability window can be represented as follows:

†A part of this paper has been presented in the 59th Battery Symposium in Japan (Presentation #1G22).
§ECSJ Active Member
§§ECSJ Fellow

K. Nakamoto orcid.org/0000-0003-4398-6597
R. Sakamoto orcid.org/0000-0003-1382-8803
M. Ito orcid.org/0000-0003-1689-446X
S. Okada orcid.org/0000-0002-8944-1990

$$E_{\text{ox, pH}} = E_{\text{OER}} + \eta_{\text{ox, conc.}} + \eta_{\text{ox, pH}} = E_{\text{ox, conc.}} - 0.059\Delta\text{pH}_{\text{cathode}} \quad (9)$$

$$E_{\text{red, pH}} = E_{\text{HER}} - \eta_{\text{red, conc.}} - \eta_{\text{red, pH}} = E_{\text{red, conc.}} - 0.059\Delta\text{pH}_{\text{anode}} \quad (10)$$

However, non-ideal aqueous solutions do not simply obey the Eqs. 9 and 10, therefore, it is practically difficult for a variety of concentrated electrolytes to estimate the unusual acidity[12] or sufficient pH gradient to resist the electrolysis of water. Several pioneering studies have reported on the relevant pH gradient for a large-scale practical cell[13] and for a divided cell.[14] Notably, the latter example provides reliable evidence for the pH gradient since ion-selective ceramics effectively prevent the crossover of H^+/OH^- between the catholyte and anolyte. However, there still remains a concern for conventional aqueous electrochemical cells such as a beaker-type cell[15] or a Swagelok-type cell,[16] which could readily allow the crossover of H^+/OH^- due to a short inter-electrode distance, and therefore, a transient pH gradient could disappear under operation.

Recently, we reported the operation of high-voltage aqueous sodium-ion batteries using concentrated electrolytes,[17,18] in which the global pH values of the electrolytes were measured at each important point during cell operation.[17] We revisited this study and monitored the local pH values continuously in the close vicinity of the cathode/anode, in order to draw a clearer picture of the merits and demerits of the transient pH gradient. We describe herein these results.

2. Experimental

2.1 Electrode preparation

Prussian blue-type (cyanoperovskite-type or hexacyanometallate-type compounds) $Na_{1.24}Mn[Fe(CN)_6]_{0.81}\cdot 1.28H_2O$ cathode (NMHCF, theoretical/practical reversible capacities are 120/116 mAh g^{-1}, respectively) and $K_{0.01}Mn[Cr(CN)_6]_{0.72}\cdot 2.01H_2O$ anode (KMHCC, theoretical/practical reversible capacities are 83/58 mAh g^{-1}, respectively) active materials were prepared by the co-precipitation method and the products were characterized by XRD, ICP-AES, and TG analysis as our previous report.[18] The active material, acetylene black (AB; DENKA), and polytetrafluoroethylene (PTFE, Polyflon F-104; Daikin Industries) were mixed in a weight ratio of 70 : 25 : 5 to prepare electrode materials, each of which was shaped into dia. 3 mm-disc pellets and sandwiched between titanium mesh (Thank-Metal). The cathode/anode weight balance was adjusted to 1/2 (0.595 mg-NMHCF/1.19 mg-KMHCC as active materials, respectively) to fix the capacity balance as approximately 1/1 based on their reversible capacities (a slight excess of anode by considering its smaller initial capacity) for aqueous sodium-ion full cells.

2.2 Electrochemical cell preparation

The aqueous electrolyte was prepared by dissolving $NaClO_4$ (98 %; Kishida) in distilled water (Direct-Q UV 3, Merck KGaA) at the concentration of 17 mol kg^{-1} (m). Galvanostatic charge-discharge tests using three-/two-electrode beaker-type cells were performed with/without an Ag-AgCl electrode in saturated KCl (RE-1CP; BAS Inc.) as the reference electrode. The short cell of ca. 1 cm inner width and ca. 4.5 mL volume was filled with 17 m $NaClO_4$ aq. (1 mL) and equipped with the cathode and anode, whose inter-electrode distance was slightly less than 1 cm. The long cell of ca. 5 cm inner width and ca. 20 mL volume was filled with 17 m $NaClO_4$ aq. (5 mL) and equipped with the cathode and anode, whose inter-electrode distance was slightly less than 5 cm. As shown in Fig. S1, the *operando* pH measurements were performed by fixing an extra-fine micro-glass electrode (dia. 3 mm, 6069-10C; HORIBA) at a distance of 5 mm from the cathode/anode surfaces, as probes of pH meter (LAQUAact D73-T; HORIBA). To confirm the influence of pH gradient in the electrolyte, the magnetic stirrer was located beneath the long cell and the stirrer bar was rotated at 600 rpm (mini stirrer; AS ONE corporation) at the middle point between the electrodes during the galvanostatic tests.

A coin-type cell (2032 type; Hohsen Corp., Fig. S2d) made of stainless steel was assembled with a non-woven separator (thickness ~ 100 µm, HT-40C; Daiwabo Polytec Co., Ltd.), which has an air permeability of 969 mL m^{-2} Pa^{-1} s^{-1} determined by Gurley-type densometer (G-B3C; Toyo Seiki Seisaku-sho Ltd.). Its surface morphology was characterized by scanning electron microscopy (SEM, JCM-7000; JEOL Ltd.) using gold sputtering (Fig. S3). Galvanostatic charge-discharge tests were carried out using a cycler (NAGANO & Co.) at a rate of 5.0 mA cm^{-2} constant current density (~5 C rate), and the interval between charge and discharge was set as 1 min unless otherwise stated.

3. Results and Discussion

3.1 Effect of the inter-electrode distance on cyclability

Our initial study began by comparing the electrochemical performance of two aqueous cells with different inter-electrode distance, in the hope that the impact of the kinetic difference in the crossover of H^+/OH^- becomes evident. Although there was no striking difference in the initial charge/discharge curves (Figs. 1a and 1b), the long cell displayed a higher discharge capacity (Fig. 1c) and more stable coulombic efficiency (Fig. 1d) than the short cell. These results convinced us that the inter-electrode distance exerts a non-negligible effect on the cell performance. We believe that a transiently yet more broadly expanded stability window may finally result in the better cyclability and the higher coulombic efficiency. Similar phenomenon has a precedent in the past.[14]

It is noteworthy that similar experiments in the coin-type cell with a non-woven separator under otherwise identical conditions resulted in a higher discharge capacity and a less stable coulombic efficiency (Figs. S2a–S2c). Although the inter-electrode distance of this coin-type cell was shorter (ca. 100 µm ≈ non-woven separator, Fig. S3), the aqueous electrolyte-absorbed non-woven separator may prevent the crossover of H^+/OH^- in the cell to maintain the expanded stability window. The inferior coulombic efficiency may arise from a possible corrosion of the stainless steel of the coin-type cell, since it was directly exposed to an aqueous electrolyte, although a complete understanding requires further study.

3.2 Relationship between cyclability and local pH during operation

To characterize the beneficial effects of a possible pH gradient on the cyclability, next we measured the in situ pH in the close vicinity of the electrodes continuously during galvanostatic cycling of the long beaker-type cell (Fig. S1). The capacity decay and the coulombic efficiency (Fig. 2a) were similar to those for the long cell without a pH meter (Figs. 1c and 1d). As illustrated in Fig. 2b, the initial pH values in the close vicinity of both electrodes were not different from the global pH ($\text{pH}_{\text{initial}} \approx 6$), but the pH values dramatically split up into strongly acidic values (ca. 1–2) at the cathode ($\text{pH}_{\text{cathode}}$) and into weakly basic values (ca. 7–8) at the anode (pH_{anode}) within several cycles after the start. These results indicate that the pH gradient developed by the water electrolysis may persist over a period long enough to maintain an expanded stability window of the electrolyte, according to the Eqs. 9 and 10, thereby allowing stable operation. By contrast, a magnetic stirring of the electrolyte at the middle point of the long cell accelerated the capacity fade and destabilized the coulombic efficiency as shown in Fig. 2c. In accordance with these results, the $\text{pH}_{\text{cathode}}$ and pH_{anode} did not split up distinctively under magnetic stirring (Fig. 2d).

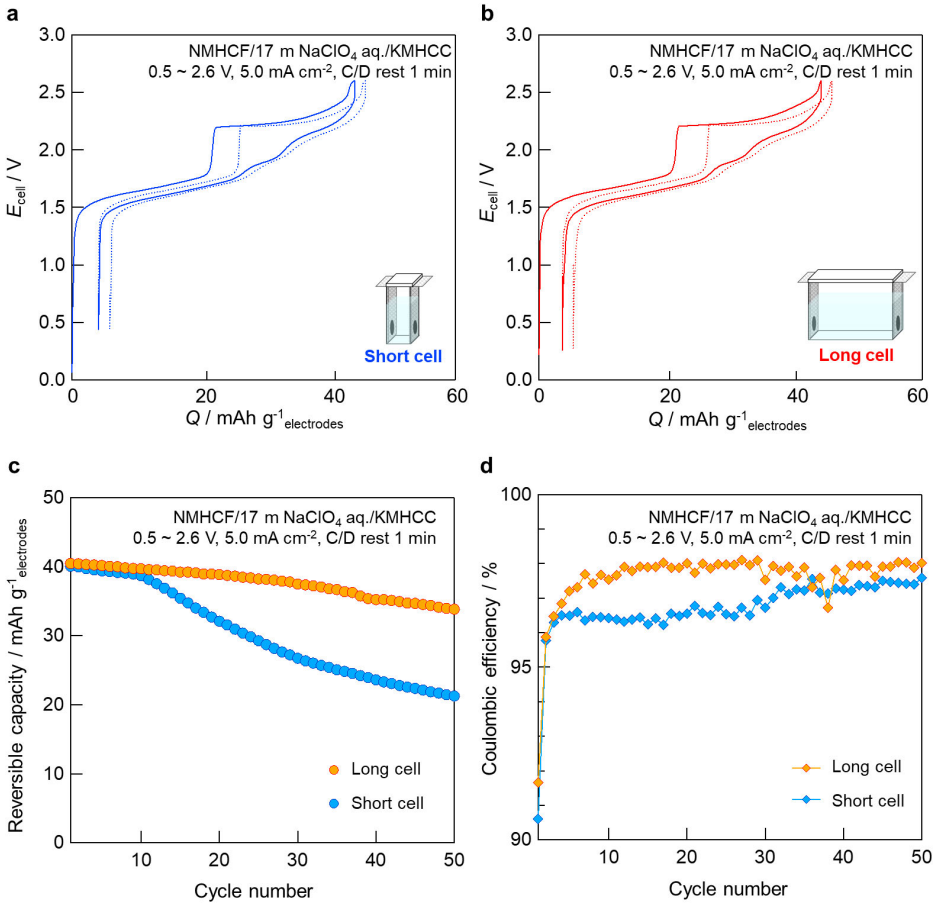

Figure 1. Typical charge/discharge profiles of the NMHCF//KMHCC beaker-type full cells with (a) short and (b) long inter-electrode distance. Comparison between the two cells in (c) cyclabilities and (d) coulombic efficiencies. The cell operation was performed without stirring of the electrolyte.

Initially, they both remained acidic within the first 1,500 min and then started to become less acidic after 1,500 min with a modest degree of split (Fig. 2d). The two discrete redox potentials in the NMHCF cathode are mainly responsible for these results as described below, although the hydronium ions stored in the as-prepared NMHCF cathode[19,20] may contribute to the acidity albeit partially. If the oxidative electrolysis of water competes primarily with the higher Mn^{II}/Mn^{III} rather than the lower Fe^{II}/Fe^{III} redox potentials, the increasing resistance should force the cell voltage to reach the cutoff faster, leave the capacity from the higher Mn^{II}/Mn^{III} redox unused, and finally almost stop the H^+ generation with concomitant O_2 evolution, as the cycles progress. On the other hand, the reductive electrolysis of water can only compete with the single Cr^{II}/Cr^{III} redox potential in the KMHCC anode, therefore, OH^- generation with concomitant H_2 evolution does not change dramatically. Such difference should underlie the pH increase around 1,500 min in Fig. 2d. Nevertheless, we may be unaware of other factors, because the difference between $pH_{cathode}$ and pH_{anode} observed in the latter period cannot reasonably be interpreted. In any case, the poorer cyclability with the short cell in Section 3.1 was attributable to the easier crossover of H^+/OH^- even with no magnetic stirring.

3.3 Self-discharge

The coulombic efficiency has proven to be highly dependent on the pH gradient between the electrodes in aqueous batteries. To verify the impact of the time interval between charge and discharge on unfavorable self-discharge, one anomalously long interval of 20-hour rest was inserted after the 11th charge to monitor the local pH as well as the potentials of the electrodes in the long three-electrode beaker-type cell. The time-course changes of $pH_{cathode}$ and pH_{anode} and of $E_{cathode}$ and E_{anode} within the period of 1,600 min are illustrated in Figs. 3a and 3b, respectively. Similar to the results in Section 3.2, the local pH values started to split from the initial values of 6, and $pH_{cathode}$ and pH_{anode} reached to ca. 1 and ca. 8–9, respectively, at the 11th cycle (Fig. 3a). These local pH values have proven to be persistent and show only slight changes toward neutralization even after the long interval of 20 h. In fact, the $pH_{cathode}$ slowly increased to ca. 3, while the pH_{anode} remained almost unchanged. Upon restart of the normal cycling with an interval of 1 min, the $pH_{cathode}$ shifted to ca. 1 again, but the pH_{anode} remained unchanged.

On the other hand, the $E_{cathode}$ and E_{anode} repeated regular up-down and down-up cycle, respectively, during the standard cycling with an interval of 1 min (Fig. 3b, Fig. S4). However, such fluctuation halted during the long interval of 20 h after the 11th charge. $E_{cathode}$ settled down to lower values than $E_{ox,conc.}$. In contrast, E_{anode} remained nearly the same as $E_{red,conc.}$ for the first half, but suddenly started increasing for the latter half. For clarity, we added background colors in Fig. 3b to indicate three types of stability window; the central light blue area is the thermodynamic stability window of the pH 6 electrolyte, the intermediate green areas are oxidative/reductive overpotentials gained by a decrease in the ratio of water molecules in 17 m $NaClO_4$ aqueous electrolyte, and the outer red/blue areas are additional potentials gained by pH shift, respectively, in 17 m $NaClO_4$ aqueous electrolyte. The borderlines separating these areas correspond to the above-mentioned E_{OER} and E_{HER}, $E_{ox,conc.}$ and $E_{red,conc.}$, and $E_{ox,pH}$ and $E_{red,pH}$, respectively. $E_{ox,conc.}$ and $E_{ox,conc.}$ were determined to be 1.54 V and −1.24 V, respectively, in our previous study.[17]

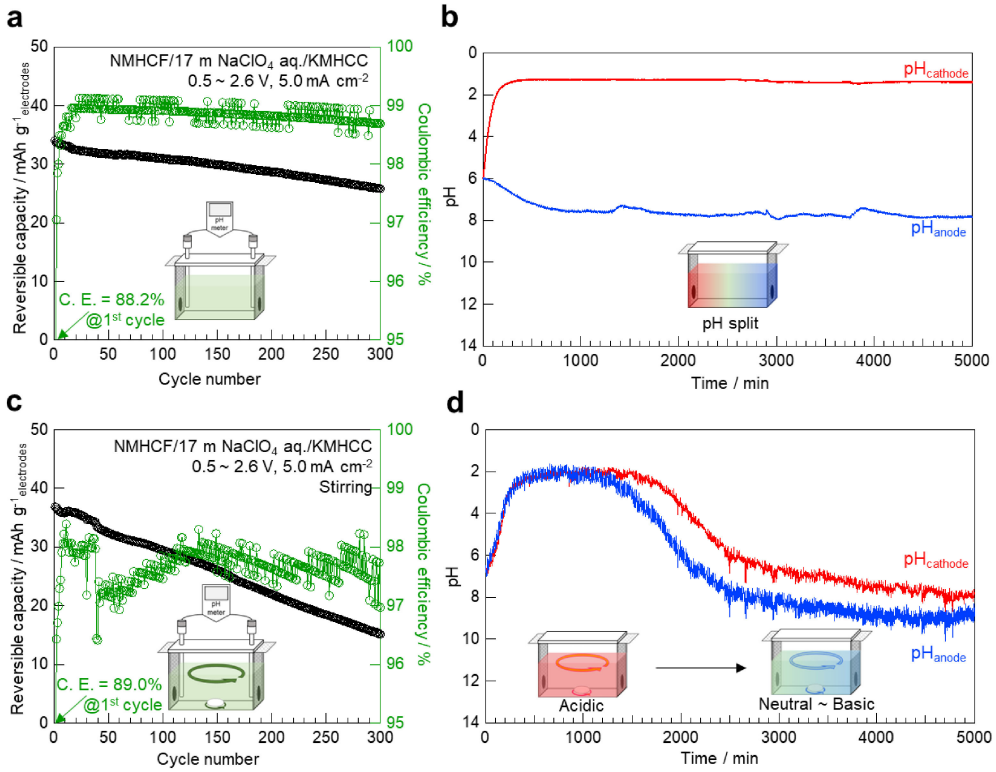

Figure 2. (a, c) Cyclabilities and (b, d) *operando* pH profiles of aqueous sodium-ion full cells. (a, b) Without stirring and (c, d) with stirring, respectively.

The difference between $E_{cathode}$ and $E_{ox,pH}$ was wider than that between E_{anode} and $E_{red,pH}$ throughout the operation including an interval of 1 min. These results suggested that the negative impact of the side reaction on the cathode was less pronounced than that on the anode. In addition, the dramatic upward shift of E_{anode} in the latter half of the long interval may indicate the oxidation of the anode. We believe that $[Cr^{II}(CN)_6]^{4-}$ in the KMHCC anode provides electrons for the reduction of water as well as dissolved O_2 to form $[Cr^{III}(CN)_6]^{3-}$ as shown in the Eqs. 11 and 12, respectively:

$$2[Cr^{II}(CN)_6]^{4-} + 2H_2O \rightarrow 2[Cr^{III}(CN)_6]^{3-} + H_2\uparrow + 2OH^- \quad (11)$$

$$4[Cr^{II}(CN)_6]^{4-} + O_2 + 2H_2O \rightarrow 4[Cr^{III}(CN)_6]^{3-} + 4OH^- \quad (12)$$

Such a self-discharge should help resist pH_{anode} neutralization. Similar phenomenon has precedents in the study of aqueous lithium-ion batteries.[21]

Figure 3c shows the capacity retention and the coulombic efficiency within the 60 cycles. The long interval after the 11th charge dramatically attenuated the charge/discharge capacities. These results may be consistent with the above-mentioned oxidation of Cr^{II} in the anode, which was further suggested by the small but steady upward shift of the cutoff potentials for the cathode/anode along with repeated cycles (Fig. S4).

The enlarged view of Fig. 3b around the 11th and 12th cycles (Fig. 3d) clearly shows that the cathode had two stepwise plateaus in the charge process of the 11th cycle (11c), whereas it became unclear in the 12th cycle (12c). These results may represent the misalignment of the state-of-charge (SOC) between the cathode and anode, because of the slight loss of cathode capacity compared to the large loss of anode capacity during 20-hour rest. This SOC misalignment severely limited the available full-cell capacity after the 12th cycle. In principle, this unfavorable SOC misalignment may be corrected by one-sided consuming the remaining capacity in the cathode. A simple and obvious method is to take an infinitely long rest time until the completion of self-discharge of the cathode in order to set both SOC to 0 %. Otherwise, a continuous operation with no unnecessarily long rest time is required to minimize the misalignment. Suitable aqueous electrolytes with larger stability windows, elimination of dissolved O_2 from the electrolyte, and/or partitioning to separate the environments around the cathode and anode may remedy this problem.

4. Conclusion

Dynamic changes in the local pH values in the close vicinity of the electrodes under high-voltage operation of aqueous batteries were identified with Prussian blue-type electrodes in a concentrated $NaClO_4$ electrolyte. A long inter-electrode distance proved to be effective in maintaining the local pH values, thereby improving the coulombic efficiency of the full cell. By contrast, the introduction of a long interval after charging may cause chemical oxidation of the anode by the reduction of water as well as the dissolved O_2 in the electrolyte, which leads to an imbalance of the remaining capacities. Our study may provide some insight into the good use of long-lasting high-voltage aqueous batteries.

Acknowledgments

This work was supported by the Elements Strategy Initiative for Catalysts and Batteries (ESICB) project (Grant Number JPMXP0112101003), JSPS KAKENHI (Grant Number JP19K15679, JP23K04910) and Japan Association for Chemical Innovation (JACI). We are grateful to Ms. Seiko Fujiwara in Kyushu University for her technical support in the pH measurements, and to Mr. Kazuhiro Shibahara and Dr. Izumi Yamada in Kyoto University for their technical support in the characterization of the non-woven separator.

CRediT Authorship Contribution Statement

Kosuke Nakamoto: Data curation (Equal), Funding acquisition (Equal), Investigation

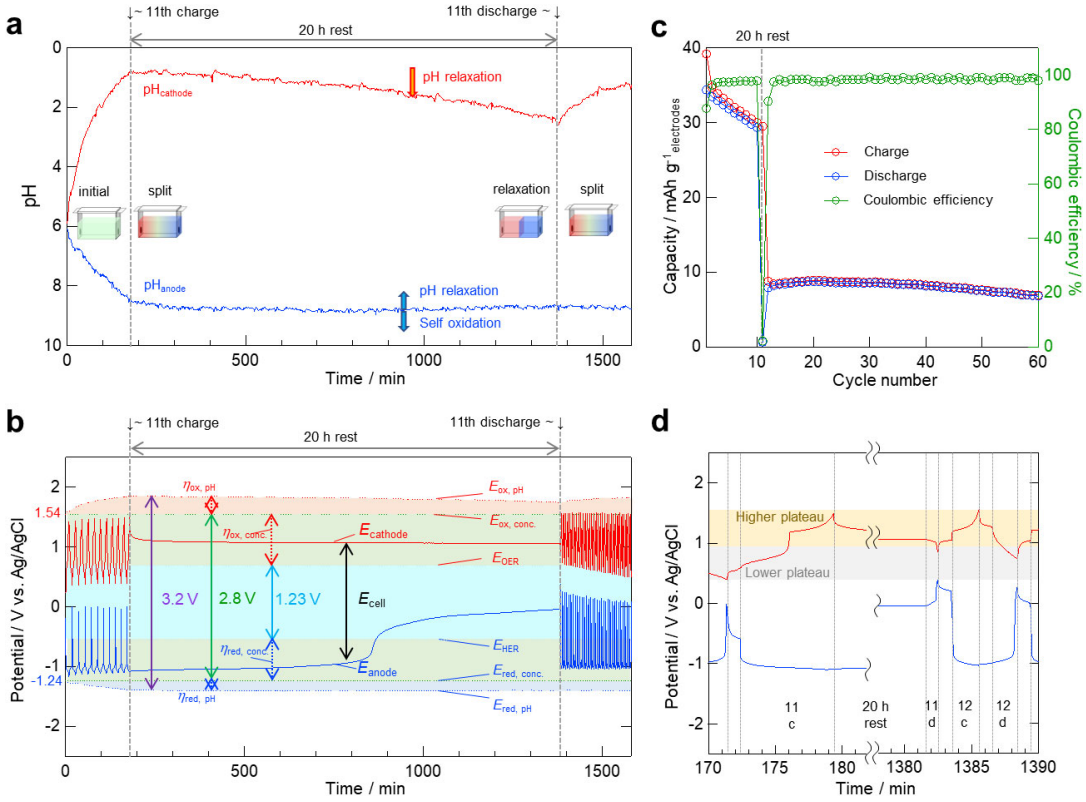

Figure 3. (a) *Operando* pH profiles of the cathode side (red solid) and anode side (blue solid) as a function of time. (b) Charge/discharge profiles of the cathode (red solid) and anode (blue solid) as a function of time in three-electrode beaker-type cell equipped with Ag/AgCl reference electrode. The central light blue area is the thermodynamic stability window of an ideal diluted aqueous electrolyte. The intermediate green areas are oxidative/reductive overpotentials caused by the concentration of the aqueous electrolyte. The outer red/blue areas are additional potentials gained by pH shift, respectively, in 17 m $NaClO_4$ aqueous electrolyte. (c) Cyclability of the aqueous sodium-ion full cell as a function of cycle numbers. (d) Enlarged view of Fig. 3b around the 11th and 12th cycles without any highlighted stability window. The cell operation was performed without stirring of the electrolyte.

(Equal), Project administration (Lead), Writing – original draft (Lead)
Miu Tanaka: Data curation (Lead), Investigation (Lead)
Ryo Sakamoto: Investigation (Supporting)
Masato Ito: Project administration (Supporting), Supervision (Equal), Writing – review & editing (Lead)
Shigeto Okada: Funding acquisition (Lead), Supervision (Lead), Writing – review & editing (Equal)

Data Availability Statement

The data that support the findings of this study are openly available under the terms of the designated Creative Commons License in J-STAGE Data listed in D1 of References.

Conflict of Interest

The authors declare no conflict of interest in the manuscript.

Funding

Japan Society for the Promotion of Science: JP19K15679
Japan Society for the Promotion of Science: JP23K04910
Ministry of Education, Culture, Sports, Science and Technology: JPMXP0112101003

References

D1. K. Nakamoto, M. Tanaka, R. Sakamoto, M. Ito, and S. Okada, *J-STAGE Data*, https://doi.org/10.50892/data.electrochemistry.24785661, (2023).
1. H. Kim, J. Hong, K. Y. Park, H. Kim, S. W. Kim, and K. Kang, *Chem. Rev.*, **114**, 11788 (2014).
2. N. Alias and A. A. Mohamad, *J. Power Sources*, **274**, 237 (2015).
3. D. Chao, W. Zhou, F. Xie, C. Ye, H. Li, M. Jaroniec, and S.-Z. Qiao, *Sci. Adv.*, **6**, eaba4098 (2020).
4. M. Liu, H. Ao, Y. Jin, Z. Hou, X. Zhang, Y. Zhu, and Y. Qian, *Mater. Today Energy*, **17**, 100432 (2020).
5. L. Suo, O. Borodin, T. Gao, M. Olguin, J. Ho, X. Fan, C. Luo, C. Wang, and K. Xu, *Science*, **350**, 938 (2015).
6. Y. Yamada, K. Usui, K. Sodeyama, S. Ko, Y. Tateyama, and A. Yamada, *Nat. Energy*, **1**, 16129 (2016).
7. J. Vatamanu and O. Borodin, *J. Phys. Chem. Lett.*, **8**, 4362 (2017).
8. N. Dubouis, P. Lemaire, B. Mirvaux, E. Salager, M. Deschamps, and A. Grimaud, *Energy Environ. Sci.*, **11**, 3491 (2018).
9. L. Droguet, A. Grimaud, O. Fontaine, and J.-M. Tarascon, *Adv. Energy Mater.*, **10**, 2002440 (2020).
10. L. Suo, D. Oh, Y. Lin, Z. Zhuo, O. Borodin, T. Gao, F. Wang, A. Kushima, Z. Wang, H.-C. Kim, Y. Qi, W. Yang, F. Pan, J. Li, K. Xu, and C. Wang, *J. Am. Chem. Soc.*, **139**, 18670 (2017).
11. D. Chao and S.-Z. Qiao, *Joule*, **4**, 1846 (2020).
12. K. S. Han, Z. Yu, H. Wang, P. C. Redfern, L. Ma, L. Cheng, Y. Chen, J. Z. Hu, L. A. Curtiss, K. Xu, V. Murugesan, and K. T. Mueller, *J. Phys. Chem. B*, **124**, 5284 (2020).
13. J. F. Whitacre, S. Shanbhag, A. Mohamed, A. Polonsky, K. Carlisle, J. Gulakowski, W. Wu, C. Smith, L. Cooney, D. Blackwood, J. C. Dandrea, and C. Truchot, *Energy Technol.*, **3**, 20 (2015).
14. H. Seki, K. Yoshima, Y. Yamashita, S. Matsuno, and N. Takami, *J. Power Sources*, **482**, 228950 (2021).
15. C. F. Bischoff, O. S. Fitz, J. Burns, M. Bauer, H. Gentischer, K. P. Birke, H.-M. Henning, and D. Biro, *J. Electrochem. Soc.*, **167**, 020545 (2020).
16. X. Liu, H. Euchner, M. Zarrabeitia, X. Gao, G. A. Elia, A. Groß, and S. Passerini, *ACS Energy Lett.*, **5**, 2979 (2020).
17. K. Nakamoto, R. Sakamoto, M. Ito, A. Kitajou, and S. Okada, *Electrochemistry*, **85**, 179 (2017).
18. K. Nakamoto, R. Sakamoto, Y. Sawada, M. Ito, and S. Okada, *Small Methods*, **3**, 1800220 (2019).
19. L. T. T. Kim, C. Gabrielli, H. Perrot, J. Garcia-Jareno, and F. Vicente, *Electrochim. Acta*, **84**, 35 (2012).
20. J. García-Jareño, A. Sanmatías, F. Vicente, C. Gabrielli, M. Keddam, and H. Perrot, *Electrochim. Acta*, **45**, 3765 (2000).
21. J.-Y. Luo, W.-J. Cui, P. He, and Y.-Y. Xia, *Nat. Chem.*, **2**, 760 (2010).